Analysis of a mesoscopic stochastic model of microtubule dynamic instability

Gennady Margolin,[1,2] Ivan V. Gregoretti,[3,2] Holly V. Goodson,[3,2] and Mark S. Alber[1,2,*]
[1]*Department of Mathematics, University of Notre Dame, Notre Dame, Indiana 46556, USA*
[2]*Interdisciplinary Center for the Study of Biocomplexity, University of Notre Dame, Notre Dame, Indiana 46556, USA*
[3]*Department of Chemistry and Biochemistry, University of Notre Dame, Notre Dame, Indiana 46556, USA*
(Received 14 April 2006; revised manuscript received 13 July 2006; published 27 October 2006)

A theoretical model of dynamic instability of a system of linear one-dimensional microtubules (MTs) in a bounded domain is introduced for studying the role of a cell edge *in vivo* and analyzing the effect of competition for a limited amount of tubulin. The model differs from earlier models in that the evolution of MTs is based on the rates of single-mesoscopic-unit (e.g., a heterodimer per protofilament) transformations, in contrast to postulating effective rates and frequencies of larger-scale macroscopic changes, extracted, e.g., from the length history plots of MTs. Spontaneous GTP hydrolysis with finite rate after polymerization is assumed, and theoretical estimates of an effective catastrophe frequency as well as other parameters characterizing MT length distributions and cap size are derived. We implement a simple cap model which does not include vectorial hydrolysis. We demonstrate that our theoretical predictions, such as steady-state concentration of free tubulin and parameters of MT length distributions, are in agreement with the numerical simulations. The present model establishes a quantitative link between mesoscopic parameters governing the dynamics of MTs and macroscopic characteristics of MTs in a closed system. Last, we provide an explanation for nonexponential MT length distributions observed in experiments. In particular, we show that the appearance of such nonexponential distributions in the experiments can occur because a true steady state has not been reached and/or due to the presence of a cell edge.

DOI: 10.1103/PhysRevE.74.041920 PACS number(s): 87.16.Ka, 82.35.−x, 05.40.−a

I. INTRODUCTION

Microtubules (MTs) are intracellular polymers which provide a part of the cytoskeleton and are responsible for many cell functions including division, organelle movement, and intracellular transport. A cell is a living object, and as such it has to constantly adjust to and communicate with a changing environment. For this purpose, MTs possess a property called dynamic instability, which enables them to promptly switch between two modes, growth and shortening [1–3]. This is achieved through MT having a stabilizing cap which keeps the MT from disassembling. The MT tends to depolymerize when the cap is lost [2–5]. The cap gradually hydrolyzes and becomes unstable as well, and so for the MT to survive it has to grow to renew its cap.

The existence of a guanosine triphosphate (GTP) cap at the end of MTs [4] and the phenomenon of dynamic instability [1] were discovered in the early 1980s. Hill and Chen used a Monte Carlo approach to simulate this behavior [2,6], employing a representation of a MT in which its cap could consist of many units (heterodimers). One of the main outcomes of their work was a suggestion that a two-phase (cap, no cap) model of dynamic instability, based only on observable macroscopic rates of phase and length changes, was sufficient to understand the behavior of the ensemble of MTs (cf. [5], Figs. 4–6). This phenomenological approach has been prevalent since then in modeling the behavior of an ensemble of MTs at the cellular level and *in vitro* [5,7–15].

In order to advance the understanding of the assembly of individual MTs, in 1990 Bayley *et al.* [16] developed the computational molecular-level lateral cap model, in which the cap consisted of a single layer of tubulin-GTP. Quite recently many computational molecular-level models of a single MT began to emerge [17–21] which try to incorporate biological details observed due to advances in the experimental techniques. In particular, it is now known from the experiments that the tips of MTs can have geometrical configurations typical to growing and shortening MTs, which differ from one another (e.g., [3]). This is closely related to the idea of the structural, and not necessarily a GTP cap [17], when due to tensile stresses inside the elastic body of a MT, its shape deforms from a cylinder near the tip.

Flyvbjerg *et al.* [22,23] introduced an elegant analytical model of the GTP cap dynamics based on a one-dimensional (linear) representation of a MT. It incorporated constitutive processes of spontaneous and vectorial hydrolyses inside the MT and fluctuating growth of the cap size. The mesoscopic scale of these processes is larger than the molecular scale, but is smaller than the scale of the phenomenological macroscopic changes. It roughly coincides with the scale of resolution of a microscope, and it allows us to define a *unit* with the length of the order of a tubulin heterodimer.

In both *in vitro* and *in vivo* experiments, the dynamics of MTs has been observed under a large variety of physical conditions and in various chemical environments. A lot of data at macroscopic scale have been accumulated including parameter values describing the MT dynamics and length distributions. Can these values be predicted based on the conditions of the experiments? How would a change in ambient conditions or the presence of spatial constraints affect observables? These questions are difficult, if not impossible, to answer using the models with postulated observable (macroscopic) rates.

In this paper we analyze a model of MT dynamics in a finite domain bounded by the cell edge, which involves competition between individual MTs for tubulin. The model is

*Electronic address: malber@nd.edu

based on a linear one-dimensional (1D) approximation of a MT structure. We consider the role of the boundary and extend the model to incorporate finite hydrolysis. Our model is different from earlier works [11,15] addressing the role of the edge in that we explicitly consider the concentration dependence of the dynamic instability parameters, as well as a competition for a limited tubulin pool. Although the cap model described in the first part of the paper deals with a single MT, the second part of the paper focuses on studying cellular level behavior of many MTs using the link between the mesoscale and the macroscale provided by the cap model.

Namely, we use a generalization of a mesoscopic model of MTs introduced in [24]. Instead of postulating macroscopic rates [2,5] or deducing them from numerical simulations [6], as was done by Hill and Chen, we estimate them analytically from basic mesoscopic rates of (de)polymerization and hydrolysis of a single unit. This results in a higher-resolution analytical model which may be more suitable for today's higher-resolution experiments and can partially address the questions posed two paragraphs above.

Recent papers [25,26] deal with modeling similar biological problems. The method of [25] is based on using macroscopic rates, while [26] does not consider finite domain size and competition for tubulin. The analyses differ as well.

There are two reasons that justify our choice of a mesoscale approach to modeling of dynamic microtubules. (i) The intermediate scale of our model is appropriate for studying the behavior of MTs at the cellular level, but without postulating the macroscopic/observable rates. (ii) A mesoscale approach is appropriate given currently available experimental data. In an ideal case, experimental results would provide a modeler with biochemical properties (such as rate constants) that determine the interactions between molecules such as tubulin. The first experimental results on microtubule dynamics at molecular resolution have been published only very recently [27]. Although these results are important, they leave several central structural questions unanswered.

The paper is organized as follows. The conceptual model and its computational implementation are presented in Sec. II. Next, in Sec. III we develop a cap model where the cap can have any number of units—see Fig. 1(b). This cap model differs from previous models in that it does not involve vectorial or induced hydrolysis. Using this model we derive approximate expressions for observable rates. We then describe in Secs. IV and V a quantitative theoretical analysis of a lower-resolution model with the cap being treated as a single unit—see Fig. 1(a). The influence of the cell edge is also studied there. Section V describes balance between polymerized and free tubulin in a bounded domain with a fixed total amount of tubulin present. Finally, we discuss and summarize our findings in Secs. VI and VII.

II. MODEL DESCRIPTION, PARAMETERS, AND NOTATIONS

In this section we describe a basic model of dynamics of MTs. We consider a domain of size $L_x \times L_y \times L_z$ with N_n available nucleation sites for MTs in its center. N_n is the maximal number of MTs—cf. Table I. For simplicity, in our study of the role of the boundary (e.g., cell edge) we assume that all MTs have an identical maximal allowed length. All MTs grow from nucleation sites (there is no spontaneous nucleation), and MTs grow at one end (usually the so-called plus end) only. There is a fixed amount of total tubulin in the domain. This tubulin is present in two forms: free tubulin in the solution and polymerized tubulin constituting the MTs. Free tubulin is taken up by growing (polymerizing) MTs and is released back into the solution by shortening MTs. In general, free tubulin (Tu) diffuses inside the domain. In this paper we assume that the diffusion of free Tu is fast and does not lead to a diffusion-limited reaction rates. This is in agreement with [28]. Moreover, we assume uniform concentration of free tubulin throughout the domain which implies instantaneous diffusion. (For studies of the effects of tubulin diffusion see [29,30].)

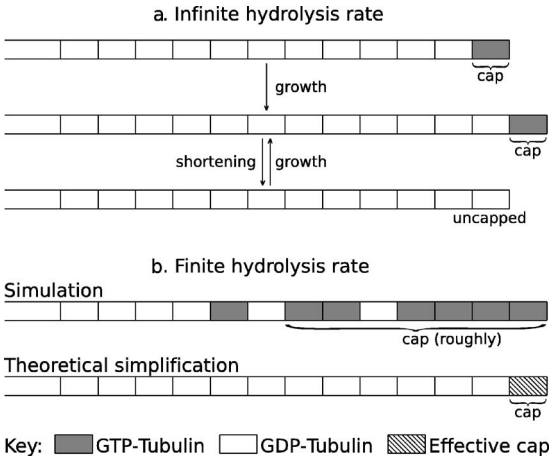

FIG. 1. Schematic representation of the model.

In this paper a MT is represented at each moment in time in the form of a 1D straight line consisting of a certain number of units of a predefined length. Each unit belonging to a MT can be in either a growth-prone state or a shortening-prone state. We will refer to them as GTP (or T) state or GDP (or D, from guanosine diphosphate) state, respectively. All free tubulin is assumed to be in a T state. When a unit joins the MT it is initially in a T state. The probability that the internal units have hydrolyzed (transformed to a D state) increases with time. When MT disassembles (shortens) these D units, upon becoming terminal, have higher probability to disassemble and return to the solution than the terminal T units. Upon return to the solution they immediately switch to the T state. The terminal T unit does not hydrolyze but can with a certain probability depolymerize (drop from MT end). Incorporation of a new unit at the MT tip triggers the hydrolysis process of the previously terminal unit. This description seems appropriate in view of [3].

The dynamics of the MTs is determined by five mesoscopic rates K_{gT} (K_{gD}) and K_{sT} (K_{sD}), which are the rates of MT growth and shortening (i.e., adding one more unit from the solution on top of the current terminal unit and losing this current terminal unit to the solution) when the terminal unit is in state T (D) and the hydrolysis rate K_h of the internal units which are in state T. If the terminal unit has to hydro-

TABLE I. Notation highlights. The dash (—) means that the considered parameter/variable is dimensionless.

Symbol	Definition	Dimensions
c	Concentration of free tubulin	μM
c_{eq}^{∞}	Critical concentration of free tubulin	μM
c_{tot}	Total concentration of tubulin	μM
k_{gT}	Second order rate of adding a unit on top of a terminal T unit	$\mu M^{-1}\, s^{-1}$
k_{gD}	Second order rate of adding a unit on top of a terminal D unit	$\mu M^{-1}\, s^{-1}$
λ	Parameter of exponential distribution (number of units)	—
ℓ	Characteristic cap size (number of units)	—
m	Mean length (number of units) of MTs	—
n	Coarsened step size in the cap model (number of units)	—
ρ	$(n-1)/(\ell-1)$	—
K_e	Rate of the edge-induced catastrophe	s^{-1}
K_h	Rate of hydrolysis (transformation to D state) of internal T units	s^{-1}
K_{gT}	Rate of adding a unit on top of a terminal T unit	s^{-1}
K_{gT}^{eff}	Effective rate of growing by one unit in growth phase	s^{-1}
K_{gT}^{obs}	Rate of growing by n units in growth phase$=K_{gT}^{eff}/n$	s^{-1}
K_{gD}	Rate of adding a unit on top of a terminal D unit	s^{-1}
K_n	Nucleation rate of a MT	s^{-1}
K_{sT}	Rate of depolymerization of terminal T unit	s^{-1}
K_{sT}^{eff}	nK_{sT}^{obs}	s^{-1}
K_{sT}^{obs}	Rate of shortening by n units in growth phase=catastrophe frequency	s^{-1}
K_{sD}	Rate of depolymerization of terminal D unit	s^{-1}
L	Maximal length (number of units) of MTs in domain with upper bound	—
L_x, L_y, L_z	Domain sizes in the numerical simulations	m
$M_g(l)$	Number of MTs of length l (number of units) in growth phase	—
$M_s(l)$	Number of MTs of length l (number of units) in shortening phase	—
N_0	Number of free nucleation seeds	—
N_{MT}	Number of MTs, $\leqslant N_n$	—
N_n	Total number of nucleation seeds	—

lyze in order to depolymerize (and its hydrolysis rate is not faster than that for the internal units), then $K_{sT}<K_h$.

For numerical simulations, shortening rates are taken to be independent of c while growth rates are assumed proportional to c at the location of MT tip:

$$K_{gT,gD}=k_{gT,gD}c. \tag{1}$$

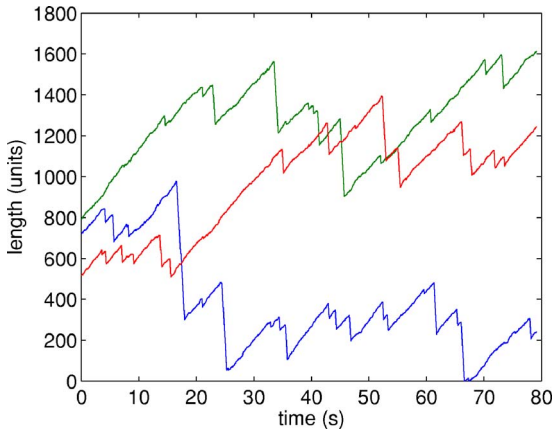

FIG. 2. (Color online) Length history plots of three arbitrarily selected MTs. Zero time here corresponds to 80 s from the start of the simulation. Here $K_h=10$, $c_{tot}=10$, and other parameters are listed in Table II. See also Fig. 5.

Such specific dependence of the growth and shortening rates on c, though, is not required for many of the theoretical results we report.

When the MT reaches boundary of the domain it is not allowed to grow anymore and will eventually lose its terminal unit initiating with certain probability a shortening phase. There are two more rates at the domain boundary of importance in the model: a rate K_n of nucleation from existing seeds and a rate K_e of edge-induced catastrophe, which can also depend on c. Appendix A contains a brief description of a numerical algorithm we used in our simulations.

In what follows, we will impose restriction on a maximal length of a MT (upper bound, e.g., due to a cell edge). We will call zero a lower bound.

Observables

The standard experimental observables describing the dynamic behavior of a single MT are derived from the MT length versus time plot. Typical length history plots of MTs are shown in Fig. 2. Due to the two-state nature of the tubulin units inside the MT, the fluctuations in this length may be large and even in the (macroscopically) steady state each MT can repeatedly change its length all the way from zero to some characteristic length or to the boundary. If no boundary is present and if free tubulin concentration stays high enough (if K_{gT} and K_{gD} are high enough), MTs can grow unbounded [7,29,31]. From a sawtoothlike evolution of a MT length four parameters can be extracted: the velocity/rate of growth, the velocity/rate of shortening, the average time of growth before switching to shortening, and the average time of shortening before switching to growth. The inverses of these times define the so-called catastrophe frequency and the rescue frequency, respectively. Note that brief growth or shortening intervals may pass unnoticed in the analysis of experimental data. Some models of dynamics of MTs use these four parameters as given constants for constructing analytical solutions [7,11] ignoring their microscopic origin. In Sec. III we use mesoscopic rates to derive the observable growth velocity and catastrophe frequency instead of setting them from the beginning.

III. CAP MODEL

Carlier and colleagues [4,32,33] have provided experimental evidence that the GTP cap of the MTs is not restricted to units at the very tip. This suggests that the hydrolysis is not instantaneous, a conclusion also supported by work on yeast tubulin [34,35]. To incorporate this feature into our approach we develop a model for the cap. In this section we show that using this model, based on the underlying mesoscopic laws, one can predict the observables: the catastrophe frequency and the velocity (rate) in the growth phase of MTs. In other words, the mesoscopic laws of the MT dynamics, governing single-unit polymerization/depolymerization and hydrolysis, can be related to the macroscale (observable) dynamics of a MT.

When $K_h < \infty$, the MT cap in our model consists mainly of T units [cf. Fig. 1(b)] and possibly of a few D units and has some characteristic length (number of units) $\ell > 1$. When $K_h \to \infty$, then $\ell = 1$ because only the terminal unit is not allowed to hydrolyze and it is in a T state. Our approach is based on coarsening the resolution in the growth phase so that only blocks of the order of cap size, $n \sim \ell$, are resolved. By catastrophe we understand the loss of the cap. In what follows we will establish a connection between coarsened "observed" rate constants $K_{gT,sT}^{obs}$ of growing or shortening *by one block of n units* (in the growth phase) and the original rates $K_{gT,sT}$ and K_h. As will become apparent from the following derivations, K_{sT}^{obs} approximates the catastrophe frequency, while nK_{gT}^{obs} is the effective rate of addition of a single unit on top of the MT, in the growth phase. There is no need to rescale $K_{gD,sD}$ if the free tubulin concentration is not too low. Therefore, we only consider a model for the MT cap and do not alter the rest.

Let us consider the cap model in detail. In what follows we neglect the fluctuations in ℓ due to randomness in hydrolysis, and we assume that each T unit is hydrolyzed after staying an internal unit for a time $\Delta t_h = 1/K_h$. After the rescue or nucleation event occurs the cap begins to grow. It has time $\Delta t_g + \Delta t_h$ to elongate, where $\Delta t_g = 1/(K_{gT} + K_{sT})$ is the time of a single-unit step in the growth phase. After that its average length remains constant (under assumption that no catastrophe occurs during this time). For the catastrophe to occur the cap should be lost, due to fluctuations in cap size and in the growth velocity [2,5,36]. In our analysis we consider two scenarios for cap loss: (i) roughly half of the cap is lost due to random nature of MTs growth, and the second half gets hydrolyzed during this time, or (ii) the whole cap is lost due to random fluctuations in MT growth. Keeping in mind that the terminal unit cannot be lost as a result of hydrolysis, in description (i) we require that $(\ell+1)/2$ and $(\ell-1)/2$ units be lost due to fluctuations in MT growth and propagation of hydrolysis front, respectively. We define

$$\rho = \frac{n-1}{\ell-1}. \tag{2}$$

In case (i) $n = (\ell+1)/2$ and $\rho = 1/2$, while in case (ii) $n = \ell$ and $\rho = 1$. It is important to stress that ρ is introduced as a fixed parameter set *a priori*, based on the scenarios of cap loss similar to (i) and (ii). The two descriptions (i) and (ii) determine the duration of the coarsened step:

$$\Delta t_g^{obs} \equiv \frac{1}{K_{gT}^{obs} + K_{sT}^{obs}} = \rho \Delta t_h + \Delta t_g \equiv \rho \frac{1}{K_h} + \frac{1}{K_{gT} + K_{sT}}. \tag{3}$$

For a given n, in order to rescale and coarsen the dynamics in the growth phase we require that both the average velocity and the diffusion coefficient of the MT tip remain unchanged, in the hypothetical case of no hydrolysis. For a random walk on a line, with probability p to jump to the right and $q = 1-p$ to jump to the left, the average velocity is $v = (p-q)\Delta x/\Delta t$ and the diffusion coefficient is $D = 2pq\Delta x^2/\Delta t$. Here Δx is the step length and Δt is the time per step. In the case of the original walk $p = p_g = K_{gT}\Delta t_g$, $\Delta x = 1$, and $\Delta t = \Delta t_g$, while in the case of the rescaled walk $p = K_{gT}^{obs}\Delta t_g^{obs}$, $\Delta x = n$, and $\Delta t = \Delta t_g^{obs}$ is given by Eq. (3). After introducing the effective rates of adding or losing one unit (as opposed to one block),

$$K_{gT,sT}^{eff} \equiv nK_{gT,sT}^{obs}, \tag{4}$$

and using conservation of v and D we obtain that

$$K_{gT}^{eff} - K_{sT}^{eff} = K_{gT} - K_{sT}, \tag{5}$$

$$\frac{K_{gT}^{eff} K_{sT}^{eff} n}{K_{gT}^{eff} + K_{sT}^{eff}} = \frac{K_{gT} K_{sT}}{K_{gT} + K_{sT}}. \tag{6}$$

From Eqs. (3) and (4), $n/(K_{gT}^{eff} + K_{sT}^{eff})$ can be found and substituted into Eq. (6), resulting in

$$K_{gT}^{eff} K_{sT}^{eff} = \beta, \tag{7}$$

where

$$\beta \equiv \frac{K_{gT} K_{sT}}{1 + \rho \dfrac{K_{gT} + K_{sT}}{K_h}}. \tag{8}$$

After solving Eqs. (5) and (7) and choosing only positive solutions we obtain that

$$K_{gT}^{eff} = \frac{K_{gT} - K_{sT} + \sqrt{(K_{gT} - K_{sT})^2 + 4\beta}}{2}, \tag{9}$$

$$K_{sT}^{eff} = \frac{-K_{gT} + K_{sT} + \sqrt{(K_{gT} - K_{sT})^2 + 4\beta}}{2}. \tag{10}$$

Expression (9) displays some expected features: namely, when

$$K_h \to \infty \Rightarrow K_{gT}^{eff} \to K_{gT}$$

and when

$$K_h \to 0 \Rightarrow K_{gT}^{eff} \to (K_{gT} - K_{sT} + |K_{gT} - K_{sT}|)/2 = \begin{cases} K_{gT} - K_{sT}, & K_{gT} \geqslant K_{sT}, \\ 0, & K_{gT} \leqslant K_{sT}. \end{cases}$$

In general, $\max(0, K_{gT} - K_{sT}) \leqslant K_{gT}^{eff} \leqslant K_{gT}$.

Equation (6) combined with Eqs. (9) and (10) yields

$$n = \frac{K_{gT}K_{sT}}{K_{gT}+K_{sT}} \frac{\sqrt{(K_{gT}-K_{sT})^2+4\beta}}{\beta}, \tag{11}$$

and Eq. (2) can now be used to determine ℓ. On the other hand, ℓ can be approximated as follows:

$$\ell \approx K_{gT}^{eff}\Delta t_h + 1 = \frac{K_{gT}^{eff}}{K_h} + 1, \tag{12}$$

where the term $K_{gT}^{eff}\Delta t_h$ approximates the number of added units after the beginning of a growth phase, before the hydrolysis front starts moving. In fact, Eq. (12) can be used as a definition of ℓ and n can be found from Eq. (2). Then there is no need for Eq. (3) as Eqs. (5), (6), and (12) form a closed set of equations. This approach, however, leads to a cubic equation for K_{gT}^{eff}, while in the above approach we need to solve a quadratic equation, which is much simpler. Nevertheless, the definition of ℓ through Eq. (12) seems to work better in the limit of $K_{gT}\to 0$. Namely, substituting Eq. (12) into Eq. (2) yields $n=1+\rho K_{gT}^{eff}/K_h$ and the only non-negative solution of this equation together with Eqs. (5) and (6), in the limit $K_{gT}\to 0$, is $K_{gT}^{eff}=0$, $K_{sT}^{eff}=K_{sT}$, and $n=1$. Indeed, it seems reasonable to postulate that $n\to 1$—i.e., there is no rescaling—when $K_{gT}\to 0$. This does not follow from Eqs. (8) and (11), which lead to $n\to 1+\rho K_{sT}/K_h > 1$ instead.

Using the above developments, it is possible to derive scaling behaviors of various quantities as functions of, e.g., c and K_h. For example, substituting Eqs. (2) and (12) into Eq. (8) and using Eq. (7) together with Eq. (4) leads to

$$K_{sT}^{obs} \approx \frac{1}{n}\frac{K_{gT}K_{sT}}{K_{gT}^{eff}+(n-1)(K_{gT}+K_{sT})} \approx \begin{cases} \dfrac{K_{sT}}{n^2}, & K_{gT} \gg K_{sT}, \\ \dfrac{K_{sT}}{2n(n-1)}, & K_{gT} \gg K_{gT}^{eff}, \end{cases} \tag{13}$$

so that the catastrophe rate (frequency) K_{sT}^{obs} scales as $n^{-2} \propto \ell^{-2}$. This is characteristic of diffusive scaling because the time to catastrophe is determined by the diffusive movement of the hydrolysis front relative to the MT tip. If the free tubulin concentration c is not too small, then Eqs. (11), (8), and (1) yield $n \propto c$ and hence $K_{sT}^{obs} \propto c^{-2}$, which is in at least qualitative agreement with previous predictions [13,37]. The scaling $K_{sT}^{obs} \propto n^{-2}$ might have been postulated, as well, which would have led us to an additional version of the solution of the cap model.

To provide another scaling example, let us now assume that K_h is small and $K_{gT} \approx K_{sT}$. Then from Eq. (8) it follows that $\beta \approx K_h K_{sT}/(2\rho) \propto K_h$. If $\beta \gg (K_{gT}-K_{sT})^2$—i.e., if K_h is not too small—then Eq. (11) yields $n \propto K_h^{-1/2}$ and hence $\ell \propto K_h^{-1/2}$ as well. Notice that it is the same scaling as derived for actin polymers [[38], Eq. (3)].

IV. ENSEMBLE DYNAMICS OF MICROTUBULES

In this section we treat the cap as a single effective unit—cf. Fig. 1. Thus the model essentially reduces to the two-phase model proposed in [5]. First, we rederive the length distribution of MTs, which are known in the literature. In particular, we study the role of upper bound (e.g., cell edge). We use these results for analyzing in the next section competition for a finite tubulin pool. We also consider the steady state critical concentration of free Tu.

In what follows, we use either the discrete or the continuous description of MT dynamics, whichever is convenient. We assume that the continuous model provides a good approximation of the discrete model. The continuous approach was discussed in [7,39,40] while an analogous discrete approach was developed in [5,11]. Following [7] we write down the equations for length distributions of MTs in growth and shortening phases in the form

$$\partial_t M_g = -K_{sT}^{obs} M_g + K_{gD} M_s - K_{gT}^{eff}\partial_l M_g, \tag{14}$$

$$\partial_t M_s = K_{sT}^{obs} M_g - K_{gD} M_s + K_{sD}\partial_l M_s, \tag{15}$$

where $M_{g,s}(l,t)$ are densities of MTs of length l at time t in the growing (g) and shortening (s) phases.

Equations (14) and (15) can be used to describe regular diffusion with drift if we do not distinguish between the phases (see also [15]). However, it is important to stress that these equations do not have diffusion terms for $M_{g,s}(l,t)$ and hence switching phases back and forth is the only mechanism of spreading of these distributions present. This is in agreement with our simulations in the case of instantaneous hydrolysis of internal units. Notice that diffusion terms are used in [5].

First, consider a semi-infinite domain. Equations (14) and (15) with the boundary condition $M_{g,s}(l=\infty)=0$ have the following steady-state solution

$$M_g = Ae^{-l/\lambda}, \tag{16}$$

$$M_s = \frac{K_{gT}^{eff}}{K_{sD}} Ae^{-l/\lambda}, \tag{17}$$

where

$$\frac{1}{\lambda} \equiv \frac{K_{sT}^{obs}}{K_{gT}^{eff}} - \frac{K_{gD}}{K_{sD}}. \tag{18}$$

The necessary condition for the existence of a steady state in the case without a boundary is given by $\lambda > 0$. The prefactor A is a normalization coefficient which depends on the total number of MT nucleation seeds present and on the nucleation probability.

We now add a constraint limiting the maximal length of MTs to be L. MTs cannot become longer due to a barrier—for example, a cell edge—as is often the case *in vivo*, especially when the cell is in the interphase and the MTs are relatively long. For simplicity we assume that L is identical for all MTs. We still can use Eqs. (14) and (15) inside the domain for $0<l<L$ and consider a steady state. Adding up these two equations then leads to $\partial_l(-K_{gT}^{eff}M_g + K_{sD}M_s)=0$, which means that the spatial derivative of the flux (of the MT tips, considered as random walkers) is zero, meaning that the flux is uniform. However, in the closed system this flux must be zero and hence

$$M_s = \frac{K_{gT}^{eff}}{K_{sD}} M_g. \tag{19}$$

It follows that Eqs. (16)–(18) still hold inside the domain, except for λ not being necessarily positive, which is in agreement with previous work [11]. This means qualitatively that there might be a steady-state distribution of MTs in which most of them are close to the upper boundary (e.g., cell edge), while only a few are short.

Critical concentration of free tubulin

Let us consider the limiting case $1/\lambda=0$ [cf. Eq. (18)]. This defines the upper limit of the concentration of free tubulin c_{eq}^{∞} at which the steady state in the semi-infinite domain still exists (cf. [7]). Let us use Eq. (1) and define

$$a = \frac{K_{sT}}{k_{gT}}, \quad b = \sqrt{\frac{K_{sT}K_{sD}}{k_{gT}k_{gD}}}. \tag{20}$$

Because the MTs in the growth phase are less likely to shorten than are MTs in the shortening phase, $a<b$. In general, $c_{eq}^{\infty} \in [a,b]$. Notice that slowdown of hydrolysis reduces $c_{eq}^{\infty}(K_h)$. When hydrolysis is instantaneous, then c reaches its maximal value $c_{eq}^{\infty}(\infty)=b$. When there is no hydrolysis at all, then $c_{eq}^{\infty}(K_h)$ reaches its minimal value $c_{eq}^{\infty}(0)=a$, meaning that the average growth rate in this case, $k_{gT}c_{eq}^{\infty}(0)-K_{sT}$, is zero.

One can get a scaling estimate of c_{eq}^{∞} if it is far enough from both a and b. Assume that $K_{gT} \gg K_{sT}$ and $K_{gT} \gg K_h$. Using Eq. (1), then $K_{gT}^{eff} \approx K_{gT} \propto c$. Now, ρ is of order of 1, so that from Eqs. (8) and (11) it follows that $\beta \sim K_{sT}K_h \ll K_{gT}^2$ and $n \sim K_{gT}/K_h \propto c/K_h$, respectively. Hence $K_{sT}^{obs} \approx K_{sT}/n^2 \propto (K_h/c)^2$. Substituting these scaling relations into $1/\lambda=0$ and using Eq. (18) yields $c_{eq}^{\infty} \propto \sqrt{K_h}$.

Notice that if there are no rescues, $k_{gD}=0$, then c_{eq}^{∞} is infinite (see also [37]) and unbounded growth cannot happen. This is so because without rescues the MT depolymerizes completely after the catastrophe, no matter how long it was before.

V. COMPETITION FOR TUBULIN

In Sec. IV we have shown the existence of a steady-state distribution of MTs inside a domain. It is conceivable that by sensing and controlling free tubulin concentration and the number of MTs the cell regulates MT dynamics, as suggested in [24,37]. In what follows we show in detail how to determine a steady-state concentration of free tubulin, c, which is the key to finding steady-state characteristics of MTs in a closed system. The main goal of this section is to derive expressions for the average number of units per MT, m, and the number of MTs, N_{MT}, as functions of c and the other parameters. These functions are needed to determine c from the conservation of total tubulin. Because m cannot extend beyond the domain boundary and because N_{MT} is less than or equal to the number of nucleation sites, N_n, the number of polymerized units in a bounded domain stays restricted as the amount of total Tu grows.

In what follows we assume that the total amount of tubulin is constant and we consider bounded domain of volume V. We also assume instantaneous diffusion so that the concentration of free tubulin is uniform throughout the domain. Hence,

$$N_{tot} = N_{free} + mN_{MT}, \tag{21}$$

where N_{tot} is a total number of tubulin units in the domain and N_{free} is a number of free tubulin units. By dividing this formula by V we obtain expression for concentrations measured in micromolars (μM):

$$c_{tot} = c + \frac{mN_{MT}}{10^{-3}N_A V}, \tag{22}$$

where V is given in m^3 and 1 μM is equal to $10^{-6}N_A$ units per liter or $10^{-3}N_A$ units per m^3; $N_A \approx 6.022 \times 10^{23}$ mol^{-1} is Avogadro's constant. We will use this expression for studying MTs in the cases of unbounded and bounded domains.

A. Unbounded domain

It has been shown in Sec. IV that the steady-state distribution of MT lengths in this case is exponential as described by Eqs. (16) and (17) with λ representing the mean length of a MT:

$$m = \lambda. \tag{23}$$

To find N_{MT} for a given N_n, we use a balance equation for the number of available nucleation sites $N_0 \equiv N_n - N_{MT}$:

$$K_{sT}^{obs}M_g(l=1) + K_{sD}M_s(l=1) = K_n N_0, \tag{24}$$

where K_n is the nucleation rate, which in general depends on c. The left-hand side of Eq. (24) describes the rate of production of available nucleation sites by completely depolymerizing MTs. The first term represents those MTs which experience a catastrophe, while the second term stands for those MTs which are already in the shortening phase. Using Eqs. (16) and (17), and assuming that $\lambda \gg 1$, yields

$$A(K_{sT}^{obs} + K_{gT}^{eff}) \approx K_n N_0. \tag{25}$$

In addition, approximating summation by integration,

$$N_{MT} = \sum_{l=1}^{\infty} [M_g(l) + M_s(l)] \approx \left(1 + \frac{K_{gT}^{eff}}{K_{sD}}\right) A\lambda, \tag{26}$$

results in

$$N_{MT} \approx \frac{N_n}{1 + \dfrac{K_{sT}^{obs} + K_{gT}^{eff}}{\lambda K_n (1 + K_{gT}^{eff}/K_{sD})}}. \tag{27}$$

Substituting Eqs. (23), (27), and (18) into Eq. (22), and using dependence of the rates on concentration c, Eq. (1), yields an equation $c_{tot}=F(c)$ at steady state. This equation relates free tubulin concentration c and total concentration c_{tot} as a function of all given parameters.

B. Bounded domain

Here again we impose limitation on the maximal possible length of MTs not to exceed L. In the case of a bounded domain a steady-state solution of Eqs. (14) and (15) can be calculated, and then m and N_{MT} are determined in a way

similar to the previous case. Notice that a steady state does exist even if $c > c_{eq}^{\infty}$. Since $0 \leq m \leq L$ and $0 \leq N_{MT} \leq N_n$ always hold, the second term in Eq. (22) is non-negative and bounded. Therefore, when c goes from 0 to ∞ so does c_{tot}. If the right-hand side of Eq. (22) monotonically increases with c, then there is a unique physically meaningful c for each c_{tot} at steady state.

It is shown in Appendix B that now

$$N_{MT} \approx \frac{N_n}{1 + \dfrac{K_{sT}^{obs} + K_{gT}^{eff}}{K_n[(1 + K_{gT}^{eff}/K_{sD})(1 - e^{-L/\lambda})\lambda + (K_{gT}^{eff}/K_e)(1 + K_{gD}/K_{sD})e^{-L/\lambda}]}} \tag{28}$$

and

$$m \approx \frac{(1 + K_{gT}^{eff}/K_{sD})\lambda[\lambda - e^{-L/\lambda}(L + \lambda)] + L(K_{gT}^{eff}/K_e)(1 + K_{gD}/K_{sD})e^{-L/\lambda}}{(1 + K_{gT}^{eff}/K_{sD})\lambda(1 - e^{-L/\lambda}) + (K_{gT}^{eff}/K_e)(1 + K_{gD}/K_{sD})e^{-L/\lambda}}. \tag{29}$$

When $\lambda > 0$ and $L \to \infty$, Eqs. (28) and (29) reduce to Eqs. (27) and (23), respectively. When $K_{gT}^{eff} \to 0$ and $K_{gD} \to 0$, then $\lambda \downarrow 0$ (so that $\lambda > 0$), $N_{MT} \to 0$, and $m \to 0$. When $K_{gT}^{eff} \to \infty$ and $K_{gD} \to \infty$, then $\lambda \uparrow 0$ (so that $\lambda < 0$), $N_{MT} \to N_n$, and $m \to L$, as expected.

VI. DISCUSSION OF THE RESULTS

A. Comparison with existing cap models

The cap model presented in this paper differs from the approaches used in [2,5,22,23]. First, we do not postulate the catastrophe frequency and growth velocity or derive them from numerical simulations, as was done in [2,5]. Instead, we analytically derive these macroscopic rates from small-scale rates (such as chemical rate constants). Second, we employ only spontaneous hydrolysis and do not use induced, or vectorial, hydrolysis; both types of hydrolysis were used in [22,23]. Our model agrees with the experimental data analyzed in [22,23] as can be seen from the main panel in Fig. 3 Specifically, the predicted dependence of the catastrophe frequency on MT growth velocity is in agreement with experimental data.

The cap dynamics in the model proposed by Flyvbjerg *et al.* [22,23] is modeled by addition of tubulin from the solution to the MT tip. This addition (polymerization) is faster than the propagation of the induced hydrolysis front (low end of the cap). Therefore, the cap length would grow infinitely were it not for the spontaneous hydrolysis at some point inside the cap. When it occurs, the cap is redefined as an interval between this spontaneous hydrolysis point and the MT tip. In this way, the average cap size can be kept constant at steady state. According to Flyvbjerg *et al.* [22,23], catastrophe occurs when this cap is lost, and it is postulated that the remaining GTP-Tu units below the cap are not capable of rescuing the MT. This assumption is made in order to allow for catastrophe to occur. Otherwise, in many cases the rescue would immediately follow the cap loss. While this picture is widely accepted, in our alternative model the picture is even simpler. We use only one type of hydrolysis, and we do not need to make any additional assumptions. In our model, there is a hydrolysis front due to spontaneous hydrolysis of old enough units (see Sec. III). The velocity of this front is governed by the *age* of the units inside the MT, and hence it is always approximately equal (with fluctuations) to the growth velocity. Faster growth velocity leads to a longer cap, reducing the catastrophe frequency.

Dilution experiments have shown that sharp reduction in the concentration of free Tu to low or zero values results in collapse of the MTs after a certain delay. Importantly, this delay is practically independent of the initial free Tu concentration [42]. Flyvbjerg *et al.* explain this phenomenon by arguing that the dilution results in domination of spontaneous hydrolysis which regulates the waiting time before the collapse. Therefore, this time is almost independent of the initial cap size. Our model yields the following simple explanation. When concentration of free Tu becomes very low, two events must occur for the cap to disappear. The terminal unit should be lost (rate K_{sT}) and the next unit should hydrolyze (rate K_h). If this next to last unit is old enough to hydrolyze then,

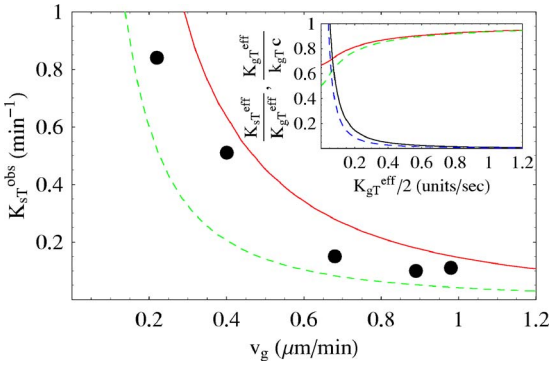

FIG. 3. (Color online) Frequency of catastrophe K_{sT}^{obs} as a function of MT growth velocity v_g. Dots represent experimental data [22,41]. Solid and dashed lines correspond to $\rho = 1/2$ and $\rho = 1$, respectively, and were obtained using the model (Sec. III). Inset: two upper curves on the right are K_{gT}^{eff}/K_{gT} and two lower curves on the right are $K_{sT}^{eff}/K_{gT}^{eff}$.

with high probability, the rest of the cap has already hydrolyzed. These events do not depend on the cap size.

Dilution experiments reported in [42] and cited in [22] determine the average waiting time before the catastrophe as roughly 5–10 s. Therefore, in Fig. 3 we set $K_h=K_{sT}=0.15\ \mathrm{s}^{-1}$. If the shortening velocity (K_{sD}) is much larger than K_{sT} and if the loss of the terminal unit is conceptualized as a two-stage process of hydrolysis and then falling, the equality $K_h=K_{sT}$ would indicate that the hydrolysis rate of the terminal unit equals the hydrolysis rate of the internal unit. Notice that we were not able to fit the catastrophe frequency data if K_{sT} and K_h were significantly different. In the dilution experiments spatial resolution was about 0.25 μm [42], which is about 30 heterodimers (per protofilament), so that actual waiting time before losing the terminal unit (heterodimer) might be faster than the reported waiting time before the collapse. We used Eq. (1) with $k_{gT}=0.3\ \mu\mathrm{M}^{-1}\ \mathrm{s}^{-1}$; however, any value of k_{gT} can be used, because it enters the formulas only through $K_{gT}=k_{gT}c$ and there is no explicit c dependence in the figure. The unit length is taken to be the length of one heterodimer of Tu, 8 nm, and hence 1 unit/s $\approx 0.5\ \mu$m/min. Therefore $v_g\ (\mu\mathrm{m/min}) \approx K_{gT}^{eff}/2$ (units/s). In the inset of Fig. 3 we show the values of $K_{sT}^{eff}/K_{gT}^{eff}$ and K_{gT}^{eff}/K_{gT}. It is seen that for $v_g>0.2$ one has $K_{sT}^{obs}<K_{sT}^{eff} \ll K_{gT}^{eff}$ and hence $v_g \propto K_{gT}^{eff} \propto c$.

B. Competition for tubulin and the edge effect

Here we study competition for a limited pool of free tubulin and combine it together with the cap model. At steady state, the dependence of the free tubulin concentration c on the total tubulin concentration c_{tot} is governed by tubulin mass conservation, Eq. (22). The resulting value of c, in turn, defines the dynamics of MTs and their ensemble distributions.

In the case of an unbounded spatial domain, we have reproduced the prediction of the Oosawa-Kasai model [43] including the existence of a critical concentration of free tubulin c_{eq}^{∞} (see thin lines in Fig. 4). The steady state cannot exist above this value. Depending on the choice of parameters, the transition from almost linear growth of c, $c \approx c_{tot}$ for low c_{tot}, to the asymptotic value $c=c_{eq}^{\infty}$ can be made sharp or smooth. (In the Oosawa-Kasai model, this transition is assumed to be sharp, meaning that when $c_{tot}<c_{eq}^{\infty}$ there are no MTs and when $c_{tot}>c_{eq}^{\infty}$ all the excess tubulin above c_{eq}^{∞} goes into polymerized state.) When the probability of rescue is zero, then $c_{eq}^{\infty} \to \infty$ and our model describes the situation considered in [37].

If there is an upper bound on MT lengths, then at sufficiently high concentrations of total tubulin, this bound inhibits further polymerization of MTs (edge effect). Hence, the steady-state free tubulin concentration can rise above its critical value. This edge effect is demonstrated by the thick lines in Fig. 4 and was first discussed in [24]. Under our reference conditions, it is seen that for $c_{tot}>20\ \mu$M the edge starts to play an important role. At sufficiently high c_{tot}, the edge reestablishes linear growth of c with respect to c_{tot}. The implications of this effect are as follows. If c_{tot} is high enough, the MTs grow persistently up until hitting the edge

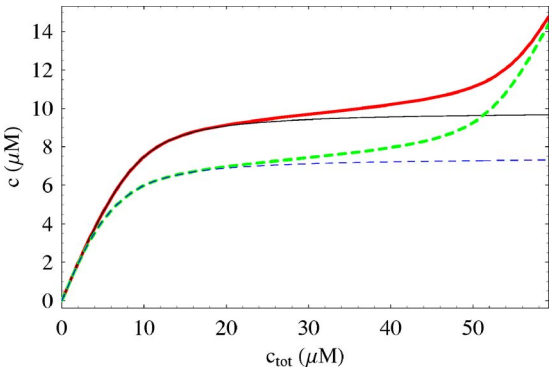

FIG. 4. (Color online) Steady-state concentration of free vs total Tu in the unbounded (thin lines) and bounded (thick lines) domains. For a bounded domain maximal MT length L is roughly 1400 units. For an unbounded domain c reaches its asymptotic value $c_{eq}^{\infty}(K_h)$. The hydrolysis rate is $K_h=10\ \mathrm{s}^{-1}$. Solid and dashed lines correspond to $\rho=1/2$ and $\rho=1$, respectively. Other parameters are $N_n=200$, $V=10^{-17}\ \mathrm{m}^3=10^{-8}\ \mu$L, $k_{gT}=5\ \mu\mathrm{M}^{-1}\ \mathrm{s}^{-1}$, $K_{sT}=5\ \mathrm{s}^{-1}$, $k_{gD}=0.5\ \mu\mathrm{M}^{-1}\ \mathrm{s}^{-1}$, $K_{sD}=500\ \mathrm{s}^{-1}$, $K_n=K_{gD}$, and $K_e=K_{sT}$, and we use Eq. (1).

which triggers their catastrophe. This is consistent with recent experimental observations of persistent growth of MTs *in vivo* [44].

From our model it follows that by changing the number of nucleation sites while keeping the total amount of Tu constant the cell could regulate the transition between mitotic (short) and interphase (long) MTs. As an example, assume $\rho=1/2$, $c_{tot}=20$, and the rest of the parameters, except N_n, as given in Fig. 4. Then $L \approx 1400$. For $N_n=50$ there are a few long MTs with $m=1100$ and $\lambda=-334$, while for $N_n=500$ there are many short MTs with $m \approx \lambda=149$. The physiological relevance of such a behavior is addressed in detail in our work [24].

Next we compare in Table II Monte Carlo simulations (see Appendix A) with the results obtained by using our continuous model. We choose large domain size so that MTs never reach the boundary and $m=\lambda$ [cf. Eq. (23)]. We run simulations for different parameter sets until steady state is reached and then determine the free tubulin concentration, number of MTs and their mean length and estimate the cap size. Recall that only MTs in growth phase have caps. Therefore, we estimate the cap size ℓ of MTs in our simulations by $\ell \sim (1+K_{gT}^{eff}/K_{sD}) \times \#T/N_{MT}$, where $\#T$ is the number of polymerized Tu units in the T state. We also use Eq. (19). For the parameter values used in Table II a simplified formula for the estimated cap size $\ell \sim \#T/N_n$ has been used.

Table II also contains theoretical estimates corresponding to the simulated values discussed above. In addition, the table includes theoretical estimates of c_{eq}^{∞} and of the cap size based on Eq. (12). In most cases the simulated results lie in between our two theoretical approximations, for $\rho=1/2$ and $\rho=1$, respectively, in agreement with the model description of cap evolution. These approximations are given as two adjacent numbers in the cells of the table displaying our theoretical estimates. When, however, K_h becomes small and c approaches a [Eq. (20)], our approximations seem to consistently overestimate the number of MTs, N_{MT}. This should

TABLE II. Comparison of simulated and theoretical results. All values reported here are at or very close to steady state. Cells containing two numbers show theoretical predictions for $\rho=1/2$ and 1, respectively. Domain size is $L_x=L_y=10^{-4}$ and $L_z=10^{-7}$ (m). It is ensured that the domain is long enough so that the MTs do not reach the boundary for the given parameters. Here $k_{gT}=5$, $K_{sT}=5$, $k_{gD}=0.5$, $K_{sD}=500$, and $K_{gT,gD}=k_{gT,gD}c$. For nucleation rate we use $K_n=K_{gD}$, i.e., a D seed, except for the third line, where it is a T seed, $K_n=K_{gT}$. $\#T/N_n$ is an estimate for the cap size—see Sec. VI B. Initially all Tu is free and its concentration is c_{tot}. Notice that $c<c_{eq}^{\infty}$.

Parameters			Simulated results				Theoretical estimates: $n=(\ell+1)/2$, $n=\ell$ (see text)					
K_h	c_{tot}	N_n	c	m	$\frac{\#T}{N_n}$	N_{MT}	c_{eq}^{∞}	c	λ	ℓ	$\frac{K_{gT}^{eff}}{K_h}+1$	N_{MT}
∞	36	2000	31.32	1416	0.759	1990	31.62	31.28	1430	1	1	1989
∞	28	3000	27.46	117	0.734	2814	31.62	27.48	112	1	1	2797
∞	28	10^4, T seed	26.48	92.7	0.780	9908	31.62	26.53	89.5	1	1	9909
10^5	36	2000	31.36	1401	0.997	1995	31.60, 31.57	31.25, 31.23	1437, 1444	1.0015	1.0016	1989
100	30	2000	20.78	2788	1.75	1992	21.05, 17.38	20.92, 17.29	2742, 3836	2.00, 1.82	2.03, 1.84	1994, 1996
30	15	2000	12.7	694	2.69	1969	14.7, 11.5	13.9, 11.2	347, 1139	3.16, 2.72	3.22, 2.77	1952, 1985
10	10	2000	7.51	758	3.94	1974	9.85, 7.48	9.02, 7.18	305, 857	5.04, 4.12	5.16, 4.20	1945, 1980
10	5	2000	4.91	35.1	2.25	1538	9.85, 7.48	4.95, 4.85	21.9, 52.1	3.06, 2.98	3.20, 3.07	1420, 1722
3	5	2000	3.94	327	5.66	1954	6.08, 4.59	4.64, 3.99	115, 312	7.22, 6.09	7.42, 6.21	1868, 1952
1	4	2000	2.56	443	8.51	1958	3.90, 2.99	3.24, 2.63	237, 420	12.5, 9.42	12.77, 9.53	1941, 1970
0.3	5	2000	1.795	971	14.0	1988	2.50, 2.00	2.31, 1.86	817, 950	23.6, 16.1	23.7, 16.1	1986, 1990
0.1	3	2000	1.379	496	19.8	1970	1.782, 1.510	1.573, 1.368	433, 494	32.1, 21.5	31.6, 20.8	1982, 1988
0.03	3	2000	1.192	553	32.9	1969	1.368, 1.234	1.262, 1.163	526, 555	50.7, 33.2	48.5, 31.1	1991, 1994
0.01	2	2000	1.080	286	42.5	1937	1.179, 1.112	1.097, 1.058	273, 284	65.6, 43.2	58.4, 37.0	1992, 1995

be improved by rescaling the rest of the rates, K_{gD}, K_{sD}, K_n, and K_e, which is outside of the scope of this paper.

C. Non-steady-state phenomena

It is often mentioned in the literature that the steady-state length distribution of MTs observed in the experiments is either exponential or bell shaped [8–10,45–47]. The exponential distribution agrees with our model. The inability to obtain a bell-shaped distribution seems to indicate a limitation to our model. While we do not exclude the possibility that some rates might depend on the MT length, as proposed by [8,9], or on the time spent in a given phase [48,49], we suggest two alternative ways of obtaining bell-shaped distributions under certain conditions. First, one should be careful in determining when the system reaches the steady state in the experiment or simulation. As our simulations demonstrate, the system reaches the constant free tubulin concentration and MTs reach the constant mean length relatively quickly. (The number of MTs does not change much henceforth.) By that time the MT length histogram is often bell shaped as illustrated in Figs. 5 and 6. This can be explained as follows. When MTs start growing from nucleation sites there is an excess of free tubulin. Therefore, the growth is originally unbounded, leading to a Gaussian shape. If the cell edge (upper boundary) is far away, in the course of this growth the free tubulin concentration drops and reaches its steady-state value. At this time the shape can still be close to a Gaussian (cf. [10] Fig. 4). This is followed by a process of a shape change of the MT length histogram with free tubulin being constant. Eventually, this results in an exponential shape and in the system reaching true steady state. The shape relaxation is relatively fast in Fig. 5, while it is very slow in Fig. 6. The shape relaxation occurs through diffusive exchange of polymer mass among the MTs, which might be orders of magnitude slower than initial rate of polymerization due to excess of free tubulin. This behavior is well described in [50,51].

A bell-shaped distribution can be also obtained in a bounded domain when the steady-state concentration of free tubulin is high enough for unbounded growth of MTs if it were not for a cell edge (i.e., if $c>c_{eq}^{\infty}$). In this situation we predict positive exponential distribution of MT lengths, in the case when all MTs can reach *identical* maximal length restricted by the edge, consistent with [11,15]. As can be seen in experiments, however, MTs are curved and cell shape is not ideally spherical or circular, so that different MTs experience different restrictions (e.g., [44,46]). This can lead to a MT length histogram of a bell-shaped form, in true steady state. Notice that in some simulations the free Tu concentration approaches its steady-state value in a nonmonotonous way—see Appendix C.

VII. CONCLUSIONS

In this paper we analyze a model of MT dynamics in a domain bounded by the cell edge which involves competition of individual MTs for tubulin. The model is based on a mesoscopic linear 1D approximation of a MT structure and includes finite hydrolysis of polymerized tubulin-GTP units.

We start by deriving analytical formulas linking mesoscopic parameters (those describing the addition, loss, and hydrolysis of individual units) to the macroscopic characteristics of a system of dynamic microtubules. Specifically, we

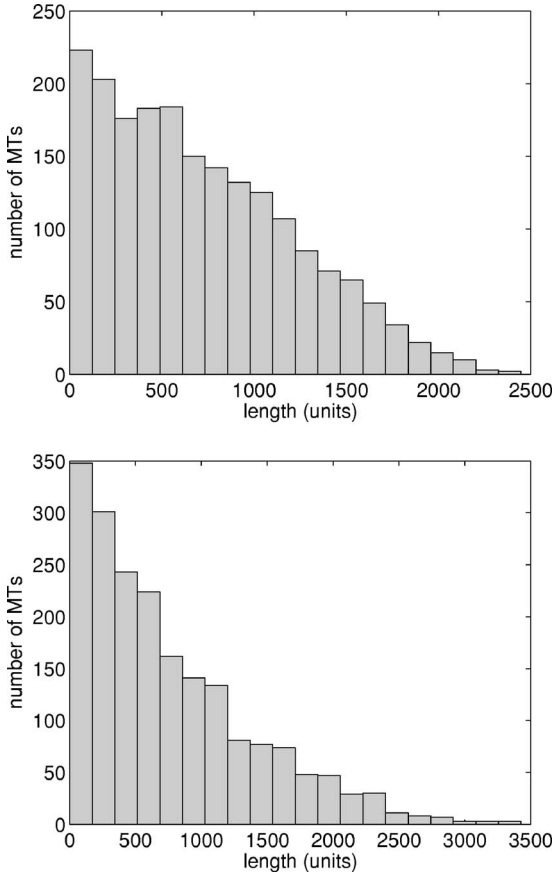

FIG. 5. Histograms of MT lengths after 80 s (top) and 160 s (bottom) from the beginning of polymerization. The concentration of free Tu in both cases is close to steady-state value: 7.63 and 7.51 μM, respectively. Although the concentration has reached steady state after 80 s, the length distribution of MTs is still changing. Here $K_h=10\ s^{-1}$, $c_{tot}=10\ \mu$M, and the rest of the parameters are specified in Table II.

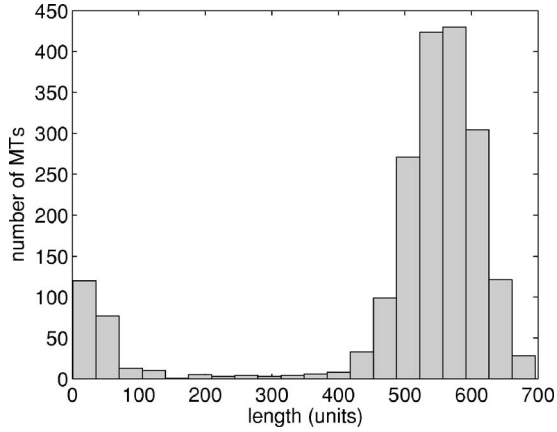

FIG. 6. Histogram of MT lengths after 150 s from the beginning of polymerization. The concentration of free Tu is 1.382 μM and has reached its steady-state value (to within random fluctuations). $K_h=0.1\ s^{-1}$, $c_{tot}=3\mu$M, and the rest of the parameters are specified in Table II. Note the bimodal character of the distribution.

are able to predict all four dynamic instability parameters: velocities of growth and shortening and frequencies of catastrophe and rescue (see Sec. III). We demonstrate how to recapitulate the macroscopic steady-state behavior of MTs using mesoscopic rates and, vice versa, extract mesoscopic rates from macroscopic behavior. Hence, it is possible to analytically and quantitatively predict the effect of changes in mesoscopic parameters on observable features, as well as to deduce mesoscopic changes from observed changes in macroscopic behavior, when relevant geometry and chemistry are taken into account.

The key ingredient in establishing a link between mesoparameters and macroparameters is the cap model, which allows one to replace the actual cap consisting of many units with an effective single unit. We demonstrate that the cap model behavior agrees with experiments measuring catastrophe frequency as a function of free tubulin concentration as well as with dilution experiments.

The model yields the following additional new results. For a cell of a given size, number of MT nuclei, and amount of total tubulin, we analyze conservation of tubulin mass equations (21) and (22) governing the balance between polymerized and free tubulin. This results in description of partitioning of tubulin, distribution of MT lengths, and macroscopic rates of the dynamic instability. We also demonstrate that, by restricting the growth of MTs, the edge can raise the free Tu concentration above its critical value for an unbounded domain, leading to a persistent MT growth inside the cell (in agreement with numerical simulations [24]). Also, an increase in nucleation activity results in an increase of the number of MTs and a decrease in their average length, reducing the edge effect. Thus, by regulating the nucleation activity, the cell can transition between interphase and mitotic arrays of MTs. These predictions can be experimentally verified.

Last, we show a very good agreement between our Monte Carlo simulations and analytical results. We also use the Monte Carlo model to provide an explanation for the nonexponential MT length distributions observed in experiments. This might be happening because of these distributions not having enough time for relaxing to an exponential shape characteristic of a steady state (see also [50,51]).

We are currently working on incorporating a molecular-level model describing individual MT protofilament structure into a unified multiscale model for investigating effects of various microtubule associated proteins (MAP's) on dynamic instability. It might be feasible to go first from the molecular to the mesoscopic level, either numerically or, perhaps, even analytically. Then, using the results of the present paper, one could go from mesoscopic to macroscopic scale and compare multiscale model predictions with experimental data at the macroscopic scale.

ACKNOWLEDGMENT

This research was supported in part by NIH Grant No. 1 RO1 GM065420: Supplement for the Study of Complex Biological Systems.

APPENDIX A: COMPUTATIONAL MODEL

In what follows we provide a short description of the numerical algorithm used for our simulations, which slightly

differs from that used in [24]. At time zero, MTs begin to grow from the nucleation seeds. At each simulation step, the time of this step is calculated by defining the rates of change in length (either growth or shortening) for each MT. If the MT tip is in T (D) state, then this rate of change is $K = K_{gT(gD)} + K_{sT(sD)}$. We demand that the maximal average number of changes for each MT will be 1, which means that we find a maximal value among all K and then set $\Delta t = 1/\max_{MTs}\{K\}$ (a technical note—we set Δt slightly below this value because the rate K for a given MT can change slightly as c is affected after each MT changes its length; these changes in c are usually very small). Then, in general, each MT will have a chance to grow, shorten, or retain its length during Δt. We do not allow a distribution of the possible number of length changes for a MT during Δt (only zero or one change is possible). After the length of each MT is updated, we update c accordingly. After updating the lengths of all MTs, the hydrolysis cycle runs through all internal units of all MTs. The probability that a unit will hydrolyze during time Δt is taken as $1-e^{-K_h \Delta t}$, assuming Poisson statistics.

All MTs have their first unit in the D state and this unit cannot be lost—this constitutes a simple nucleation seed with lower growth probability than when the MT tip is in the T state (these units are not counted when calculating the lengths of the MTs). Similarly, when the edge is relevant we can assume $K_e = K_{sT}$. Such choices are made purely to reduce the number of parameters in the system and are not essential for our purposes.

APPENDIX B: EXPLICIT SOLUTION IN THE BOUNDED DOMAIN

In what follows we obtain expressions for N_{MT} and m in the bounded domain at the steady state. Notice that in our model all the MTs of maximum length L are technically in the growing phase, because their terminal unit can never become internal and therefore does not hydrolyze. (These MTs cannot grow because of the edge.) The edge-induced catastrophe rate K_e will be governed by the smallest of the rates K_{sT} and K_h. The discrete version of Eqs. (14) and (15) determining a steady state at the boundary,

$$0 = -K_e M_g(L) + K_{gD} M_s(L-1) + K_{gT}^{eff} M_g(L-1), \quad \text{(B1)}$$

$$0 = K_e M_g(L) - K_{gD} M_s(L-1) - K_{sD} M_s(L-1). \quad \text{(B2)}$$

After summing up these two equations we recover

$$M_s(L-1) = (K_{gT}^{eff}/K_{sD}) M_g(L-1), \quad \text{(B3)}$$

which is already known [cf. Eq. (19)] and so one of these equations is superfluous. Another way to find $M_{g,s}$ is to write a general solution of Eqs. (14) and (15), $M_g = Ae^{-z/\lambda} + B$ and $M_s = (K_{gT}^{eff}/K_{sD}) Ae^{-z/\lambda} + (K_{sT}^{obs}/K_{gD}) B$, and plug it into Eq. (B3), yielding $B=0$, unless $(K_{sT}^{obs} K_{sD})/(K_{gT}^{eff} K_{gD}) = 1$, in which case B is arbitrary. But this last condition implies $\lambda \to \infty$ and hence $M_{g,s}$ are constant inside the domain. At the lower domain boundary, Eq. (24) still holds.

The number of MTs is given now by

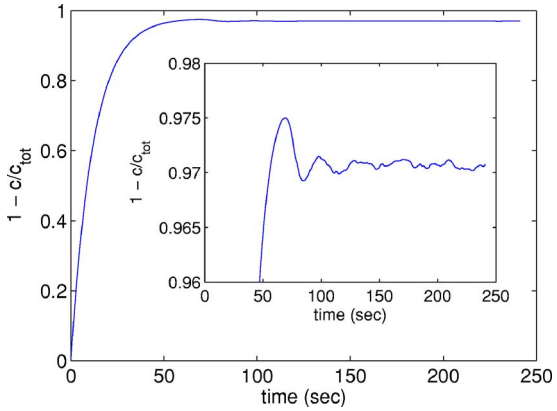

FIG. 7. (Color online) Small oscillations in the amount of polymerized Tu observed in numerical simulations for $K_h = 0.1\ \mathrm{s}^{-1}$, $c_{tot} = 50\ \mu\mathrm{M}$, and $N_n = 10^4$. Other parameters are as in Table II. The inset is a blowup of the region of oscillations.

$$N_{MT} = \sum_{l=1}^{L-1} [M_g(l) + M_s(l)] + M_g(L) = N_n - N_0. \quad \text{(B4)}$$

Using Eqs. (16), (17), (24), and (B1) and replacing the summation by the integration from 0 to L we can determine A and hence N_{MT}, which is given in Eq. (28).

Similarly, the mean MT length is

$$m = \frac{\sum_{l=1}^{L-1} l[M_g(l) + M_s(l)] + LM_g(L)}{\sum_{l=1}^{L-1} [M_g(l) + M_s(l)] + M_g(L)}, \quad \text{(B5)}$$

leading to Eq. (29).

APPENDIX C: OSCILLATIONS

In some of the simulations we observed an overshoot in free Tu concentration before the steady state was reached. Moreover, in some cases there were *slight* oscillations of free Tu concentration, as shown in Fig. 7. Overshoots and *large* oscillations have been reported and modeled in the literature [9,12,30,52–56]. It is believed that slow conversion of D- into T-tubulin in solution, after the depolymerization, is the key to understanding of such oscillations. These oscillations occur if the initial free Tu concentration is sufficiently large.

Free D-tubulin cannot polymerize. In our model we assume its conversion into T-tubulin to be instantaneous. We also use a linear (and not higher order) dependence of the nucleation rate of the free Tu concentration and a fixed number of nucleation sites. It is remarkable that under these restrictive assumptions the model produced some oscillations. We suggest the following explanation for their existence, which is in agreement with [54]. If the hydrolysis is slow enough, the MTs grow quickly in the beginning, resulting in a large cap. When the free Tu concentration changes quickly, the cap needs a relatively long time to adjust. This leads to a delayed response and possibly to oscillations. Hence it might be that the ability to produce oscillations is inherent to MT structure and that it can be magnified under certain experimental conditions.

[1] Tim Mitchison and Marc Kirschner, Nature (London) **312**, 237 (1984).
[2] Terrell L. Hill and Yi der Chen, Proc. Natl. Acad. Sci. U.S.A. **81**, 5772 (1984).
[3] Joe Howard and Anthony A. Hyman, Nature (London) **422**, 753 (2003).
[4] Marie-France Carlier and Dominique Pantaloni, Biochemistry **20**, 1918 (1981).
[5] Terrell L. Hill, Proc. Natl. Acad. Sci. U.S.A. **81**, 6728 (1984).
[6] Yi der Chen and Terrell L. Hill, Proc. Natl. Acad. Sci. U.S.A. **82**, 1131 (1985).
[7] Marileen Dogterom and Stanislas Leibler, Phys. Rev. Lett. **70**, 1347 (1993).
[8] H. Bolterauer, H.-J. Limbach, and J. A. Tuszyński, J. Biol. Phys. **25**, 1 (1999).
[9] H. Bolterauer, H.-J. Limbach, and J. A. Tuszyński, Bioelectrochem. Bioenerg. **48**, 285 (1999).
[10] N. R. Gliksman, R. V. Skibbens, and E. D. Salmon, Mol. Biol. Cell **4**, 1035 (1993).
[11] Bindu S. Govindan and William B. Spillman, Jr., Phys. Rev. E **70**, 032901 (2004).
[12] Peter M. Bayley, Maria J. Schilistra, and Stephen R. Martin, J. Cell. Sci. **93**, 241 (1989).
[13] Yi der Chen and Terrell L. Hill, Proc. Natl. Acad. Sci. U.S.A. **82**, 4127 (1985).
[14] Karl F. Freed, Phys. Rev. E **66**, 061916 (2002).
[15] Ivan V. Maly, Bull. Math. Biol. **64**, 213 (2002).
[16] Peter M. Bayley, Maria J. Schilistra, and Stephen R. Martin, J. Cell. Sci. **95**, 33 (1990).
[17] Imre M. Jánosi, Denis Chrétien, and Henrik Flyvbjerg, Biophys. J. **83**, 1317 (2002).
[18] Vincent VanBuren, David J. Odde, and Lynne Cassimeris, Proc. Natl. Acad. Sci. U.S.A. **99**, 6035 (2002); **101**, 14989(E) (2004).
[19] Vincent VanBuren, Lynne Cassimeris, and David J. Odde, Biophys. J. **89**, 2911 (2005).
[20] Evgeny B. Stukalin and Anatoly B. Kolomeisky, J. Chem. Phys. **121**, 1097 (2004).
[21] Maxim I. Molodtsov, Elena A. Ermakova, Emmanuil E. Shnol, Ekaterina L. Grishchuk, J. Richard McIntosh, and Fazly I. Ataullakhanov, Biophys. J. **88**, 3167 (2005).
[22] Henrik Flyvbjerg, Timothy E. Holy, and Stanislas Leibler, Phys. Rev. Lett. **73**, 2372 (1994).
[23] Henrik Flyvbjerg, Timothy E. Holy, and Stanislas Leibler, Phys. Rev. E **54**, 5538 (1996).
[24] Ivan V. Gregoretti, Gennady Margolin, Mark S. Alber, and Holly V. Goodson, J. Cell. Sci. (to be published).
[25] Albertas Janulevicius, Jaap van Pelt, and Arjen van Ooyen, Biophys. J. **90**, 788 (2006).
[26] Chenghang Zong, Ting Lu, Tongye Shen, and Peter G. Wolynes, Phys. Biol. **3**, 83 (2006).
[27] J. W. J. Kerssemakers, E. L. Munteanu, L. Laan, T. L. Noetzel, M. E. Janson, and M. Dogterom, Nature (London) **442**, 709 (2006).
[28] David J. Odde, Biophys. J. **73**, 88 (1997).
[29] M. Dogterom, A. C. Maggs, and S. Leibler, Proc. Natl. Acad. Sci. U.S.A. **92**, 6683 (1995).
[30] P. A. Deymier, Y. Yang, and J. Hoying, Phys. Rev. E **72**, 021906 (2005).
[31] Deborah Kuchnir Fygenson, Erez Braun, and Albert Libaber, Phys. Rev. E **50**, 1579 (1994).
[32] Ronald Melki, Marie-France Carlier, and Dominique Pantaloni, Biochemistry **29**, 8921 (1990).
[33] Ronald Melki, Stéphane Fievez, and Marie-France Carlier, Biochemistry **35**, 12038 (1996).
[34] Ashley Davis, Carleton R. Sage, Cynthia A. Dougherty, and Kevin W. Farrell, Science **264**, 839 (1994).
[35] Cynthia A. Dougherty, Richard H. Himes, Leslie Wilson, and Kevin W. Farrell, Biochemistry **37**, 10861 (1998).
[36] David J. Odde, Helen M. Buettner, and Lynne Cassimeris, AIChE J. **42**, 1434 (1996).
[37] T. J. Mitchison and M. W. Kirschner, Cell Biophys. **11**, 35 (1987).
[38] Dimitrios Vavylonis, Qingbo Yang, and Ben O'Shaughnessy, Proc. Natl. Acad. Sci. U.S.A. **102**, 8543 (2005).
[39] T. L. Hill, *Linear Aggregation Theory in Cell Biology* (Springer-Verlag, New York, 1987).
[40] Fulvia Verde, Marileen Dogterom, Ernst Stelzer, Eric Karsenti, and Stanislas Leibler, J. Cell Biol. **118**, 1097 (1992).
[41] D. N. Drechsel, A. A. Hyman, M. H. Cobb, and M. W. Kirschner, Mol. Biol. Cell **3**, 1141 (1992).
[42] R. A. Walker, N. K. Pryer, and E. D. Salmon, J. Cell Biol. **114**, 73 (1991).
[43] F. Oosawa and M. Kasai, J. Mol. Biol. **4**, 10 (1962).
[44] Yulia A. Komarova, Ivan A. Vorobjev, and Gary G. Borisy, J. Cell. Sci. **115**, 3527 (2002).
[45] Neal R. Gliksman, Stephen F. Parsons, and E. D. Salmon, J. Cell Biol. **119**, 1271 (1992).
[46] Lynne U. Cassimeris, Patricia Wadsworth, and E. D. Salmon, J. Cell Biol. **102**, 2023 (1986).
[47] Fulvia Verde, Jean-claude Labbé, Marcel Dorée, and Eric Karsenti, Nature (London) **343**, 233 (1990).
[48] David J. Odde, Lynne Cassimeris, and Helen M. Buettner, Biophys. J. **69**, 796 (1995).
[49] David J. Odde and Helen M. Buettner, Biophys. J. **75**, 1189 (1998).
[50] Ben O'Shaughnessy and Dimitrios Vavylonis, Phys. Rev. Lett. **90**, 118301 (2003).
[51] B. O'Shaughnessy and D. Vavylonis, Eur. Phys. J. E **12**, 481 (2003).
[52] M. F. Carlier, R. Melki, D. Pantaloni, T. L. Hill, and Y. Chen, Proc. Natl. Acad. Sci. U.S.A. **84**, 5257 (1987).
[53] Yi der Chen and Terrell L. Hill, Proc. Natl. Acad. Sci. U.S.A. **84**, 8419 (1987).
[54] Elmar Jobs, Dietrich E. Wolf, and Henrik Flyvbjerg, Phys. Rev. Lett. **79**, 519 (1997).
[55] D. Sept, Phys. Rev. E **60**, 838 (1999).
[56] D. Sept and J. A. Tuszyński, J. Biol. Phys. **26**, 5 (2000).